A tumor-penetrating peptide modification enhances the antitumor activity of endostatin *in vivo*

Zhang Hai-Tao[a,b], Li Hui-Cheng[b], Li Zheng-Wu[b] and Guo Chang-Hong[a]

Many antitumor drugs have a limited ability to penetrate more than a few cell diameters from blood vessels into solid tumors, which limits their effectiveness. In this study, we investigated whether the biological activity of endostatin can be enhanced by the addition of an integrin-targeting and permeability-enhancing sequence. The internalization RGD (CRGDKGPDC; iRGD) sequence was added at the carboxyl terminus of endostatin. Modification of endostatin with the iRGD motif showed specific and increased binding to endothelial cells; the increased binding correlated with an improved antiangiogenic property. iRGD-modified endostatin was more effective than human endostatin in inhibiting liver cancer growth in athymic mice. The finding indicates that addition of a vascular targeting and permeability sequence can enhance the biological activity of an antiangiogenic molecule and tumor targeting. *Anti-Cancer Drugs* 22:409–415 © 2011 Wolters Kluwer Health | Lippincott Williams & Wilkins.

Anti-Cancer Drugs 2011, **22**:409–415

Keywords: angiogenesis, antiangiogenesis, endostatin, endothelial cell, integrin, RGD ligands, tumor targeting

[a]Key Laboratory of Molecular Cytogenetics and Genetic Breeding of Heilongjiang Province, College of Life Science and Technology, Harbin Normal University and [b]Harbin Pharmaceutical Group R&D Center, Harbin, China

Correspondence to Guo Chang-Hong, Key Laboratory of Molecular Cytogenetics and Genetic Breeding of Heilongjiang Province, College of Life Science and Technology, Harbin Normal University, Harbin 150025, China
Tel: +86 13 936622308; fax: +86 045188060673;
e-mail: kaku3008@yahoo.com.cn

Received 3 August 2010 **Revised form accepted** 28 October 2010

Introduction

Endostatin, the C terminal fragment of collagen XVIII with a molecular weight of 20 kDa, has been approved by the State Food and Drug Administration of China for its anticancer activity. It specifically inhibits endothelial cell proliferation and migration, and reduces vascularization and blood flow in gliosarcoma [1]. It dramatically inhibits the growth of various primary tumors in mice as well. Endostatin has been shown to be a potent antiangiogenic protein and may target integrins, which are cell surface receptors that are important for the migration and invasion of tumor cells [2–5], and its antitumor property has been confirmed in more than 980 publications listed in Pubmed [5]. In addition, the protein does not cause toxicity in patients [6,7].

The therapeutic efficacy of many anticancer drugs, including endostatin, is limited by their poor permeability in tumor tissue. In addition, their adverse effects on healthy cells limit the dose of drug that can be safely administered to patients with cancer. In solid tumors, many anticancer drugs penetrate only 3–5 cell diameters from the blood vessels, leading to a reduced efficacy and development of drug resistance [8]. For some years, it has been known that peptides containing the RGD (Arg-Gly-Asp) sequence recognize integrins, and these peptides have been used for homing to malignant tissue. Recent studies have identified the tumor-penetrating peptide internalization RGD (iRGD; sequence CRGDK/RGPD/EC) [9]. Conjugation of iRGD with a drug can facilitate the penetration of the iRGD into extravascular tumor tissue [10]. Similar to conventional RGD peptides, the intact peptide binds to the surface of cells expressing av integrins that are specifically expressed on the endothelium of tumor vessels [8,10,11], where it is proteolytically cleaved to produce the CRGDK/R fragment. This fragment then binds to neuropilin-1 (NRP-1) and penetrates into tumor cells and tissues. The truncated peptide loses much of its integrin-binding activity, but gains affinity for NRP-1 because of the C terminal exposure of a conditional C end Rule motif (R/KXXR/K) [9]. The NRP-1 binding triggers tissue penetration, which is tumor specific, because the cleavage requires previous binding of the peptide to integrins [12]. These features confer on iRGD a tumor-specific tissue penetration activity.

We hypothesized that by introducing the iRGD sequence into human endostatin, its tumor-specific tissue penetration activity would be improved, and thus increases the antitumor effect. In this study, the iRGD sequence was conjugated to the C terminus of endostatin by the GGGGS linker sequence, through bioengineering methods in *E. coli* expressing the recombinant protein. Using cell-attachment assay, cell-proliferation experiments, cell-migration assay, chorioallantoic membrane assay (CAM), and in-vivo antitumor experiments, we confirmed that iRGD endostatin has stronger antiangiogenic and antitumor activity than human endostatin without the conjugated iRGD.

Materials and methods

Cloning, expression, and purification of iRGD–endostatin fusion protein

Human endostatin cDNA and iRGD (CRGDKGPDC) cDNA were linked to each other through a DNA sequence coding to form a 5-mer linker (GGGGS) peptide, the iRGD–endostatin fusion protein. Plasmid pET-3a-endostatin-G_4S-iRGD was constructed by PCR.

0959-4973 © 2011 Wolters Kluwer Health | Lippincott Williams & Wilkins DOI: 10.1097/CAD.0b013e328342050d

The DNA fragment encoding endostatin–linker–iRGD was amplified from pET-32a-endostatin by PCR with primers P1 and P2. The PCR was performed using the following amplification conditions: an initial denaturing step at 94°C for 3 min, 30 cycles at 94°C for 45 s, 56°C for 40 s, 72°C for 1 min, and a final extension at 72°C for 10 min. The amplified products were digested with NdeI and BamHI and inserted into the same digested pET-3a to obtain pET-3a-endostatin-G_4S-iRGD fusion plasmid. The primers used in this procedure were as follows:

P1: CATATGATGCATAGCCATCGTGATTTTCAGCC GGTGCTG (NdeI site is underlined)
P2: GGATCCGCAATCCGGGCCTTTATCGCCACGG CAGCTGCCGCCGCCACCTTTGCTCGCGGTCATAA AGGTATT (BamHI site is underlined)

Fusion protein sequence: CATAGCCATCGTGATTTT CAGCCGGTGCTGCATCTGGTGGCGCTGAACAGC CCGCTGAGCGGCGGCATGCGTGGCATTCGTGGC GCGGATTTTCAGTGCTTTCAGCAGGCGCGTGCG GTGGGCCTGGCGGGCACCTTTCGTGCGTTTCTG AGCAGCCGTCTGCAGGATCTGTATAGCATTGTGC GTCGTGCGGATCGTGCGGCGGTGCCGATTGTGA ACCTGAAAGATGAACTGCTGTTTCCGAGCTGGGA AGCGCTGTTTAGCGGCAGCGAAGGCCCGCTGAAA CCGGGCGCGCGTATTTTTAGCTTTGATGGCAAAG ATGTGCTGCGTCATCCGACCTGGCCGCAGAAAAG CGTGTGGCATGGCAGCGATCCGAACGGCCGTCGT CTGACCGAAAGCTATTGCGAAACCTGGCGTACCG AAGCGCCGAGCGCGACCGGCCAGGCGAGCAGCCT GCTGGGCGGCCGTCTGCTGGGCCAGAGCGCGGC GAGCTGCCATCATGCGTATATTGTGCTGTGCATT GAAAACAGCTTTATGACCGCGAGCAAAGGCGGCG GCGGCAGCTGCCGTGGCGATAAAGGCCCGGATTGC.

E. coli BL21 (DE3) cells containing the recombinant plasmid were grown at 37°C in M9 + LB medium (3.6 l) supplemented with ampicillin (0.5 g), $MgSO_4$ (1.2 g), and antiblowing agent (1 ml). When OD600 reached 6, 0.6 g of isopropyl β-D-1-thiogalactopyranoside was added to induce the expression of the fusion proteins. After a further 5 h of cultivation, the cells were harvested and subjected to sonication. The inclusion bodies thus obtained were washed three times with Tris/HCl (20 mmol/l; pH 8.2) and 0.5% (v/v) of Triton X-100 and then dissolved in a denaturing buffer [guanidine–HCl (6 mol/l), ethylenediaminetetraacidic acid (EDTA; 5 mmol/l), dithiothreitol (10 mmol/l), and Tris/HCl (20 mmol/l), pH 8.2]. The denaturing liquid was subjected to slow dilution into the refolding buffer [urea (2 mol/l), Tris/HCl (20 mmol/l), and glutathione disulfide (0.25 mmol/l), pH 8.5] by a volume ratio of 1 : 100 at 4°C. This was left standing for 20 h, and then was ultrafiltrated to one-tenth of the total volume through ultrafilters with pore-size membranes of 10 kDa. Subsequently, the protein solution was loaded onto a Phenyl, SP, Q-Sepharose Fast Flow chromatographic column (Pharmacia, sweden). Elution of the fusion proteins was performed with a salt concentration of 0.3 mol/l of NaCl in 20 mmol/l of Tris/HCl, pH8.0. The eluted fusion protein fractions were analyzed by SDS-polyacrylamide gel electrophoresis (PAGE) and western blot.

Cell-attachment assay

A measure of 1 nmole per well endostatin or iRGD-modified endostatin and 0.2% gelatin was used to coat 96-well polystyrene plates. The plates were incubated at 4°C overnight and then blocked with 2% of bovine serum albumin in phosphate buffer solution (PBS) at 37°C for 2 h. Human umbilical vein endothelial cells (HUVECs), MA148 (negative control), or WM35 (positive control for $\alpha_v\beta_3$ integrin-expressing cell line) were harvested in PBS-containing EDTA (1 mmol/l) and prelabeled for 10 min at 37°C with 5-(and-6)-carboxyfluorescein diacetate (5 μmol/l), succinimidyl ester (CFDA/SE), a fluorescent dye (Invitrogen, Carlsbad, California, USA). After washing with Hank's balanced salt solution, fluorescence-labeled cells were resuspended in endothelial growth media (i.e. HUVECs culture medium) or Roswell Park Memorial Institute-1640 medium supplemented with 10% fetal bovine serum (FBS; MA148, WM35). The cells were incubated with or without competitors including 1 μg of anti-$\alpha_v\beta_3$ integrin monoclonal antibody (Univ-bio, Shanghai, China) and 1 μl of anti-$\alpha_5\beta_1$ integrin monoclonal antibody (Univ-bio) for 1 h at 37°C. Cells were then added to wells at a density of 40 000 cells per well (HUVECs and MA148) or 30 000 cells per well (WM35). After 1-h incubation at 37°C, plates were washed twice with Hank's balanced salt solution to remove unbound cells. Cells bound to the wells were assayed with a fluorescence plate reader (BioRad; Hercules, California, USA) (excitation, 485 nm; emission, 530 nm).

Endothelial cell-proliferation assay

Bovine capillary endothelial cells were obtained from the American Type Culture Collection (Manassas, Virginia, USA). For the proliferation assay, cells were washed with PBS and dispersed in a 0.05% of trypsin solution. A cell suspension (25 000 cells/ml) was made with Dulbecco's modified Eagle medium (DMEM) + 10% FBS + 1% F-12, plated onto gelatinized 24-well culture plates (0.5 ml/well), and incubated (37°C, 5% CO_2) for 24 h. The media was replaced with 0.25 ml of DMEM + 5% FBS + 1% F12 and the test samples were applied (iRGD-modified endostatin and endostatin). After 20 min of incubation, media and basic fibroblast growth factor (bFGF) were added to obtain a final volume of 0.5 ml of DMEM + 5% FBS + 1% F12 + 5 ng/ml bFGF. After 72 h, cells were dispersed in trypsin, resuspended in isotonic-buffered saline (Sigma Chemicals, St Louis, USA), and counted by the (3-(4,5-dimethylthiazol-2-yl)-2, 5-diphenyltetrazolium bromide method.

Endothelial cell-migration assay

The migration of endothelial cells was determined by using transwell chambers (Costar, Shanghai, China).

Polycarbonate filters (pore size of 12 μm) were coated with 0.2% gelatin for 1 h at 37°C. HUVECs were harvested in EDTA (2 mmol/l) in PBS and prelabeled with CFDA/SE (5 μmol/l) for 10 min at 37°C. Cells were resuspended in 0.5% FBS + M199 medium and then preincubated with iRGD-modified endostatin or endostatin for 60 min at 37°C. Vascular endothelial growth factor (VEGF; 25 μl of 25 ng/ml of FGF within 0.5% FBS + M199 medium) was added to the lower chambers. HUVECs (200 000 cells/ml, control and treated) were added to upper chambers. After 4 h of incubation at 37°C, endothelial cells that had migrated to the bottom side of the membrane were counted in a fluorescence microscope (Olympus, Tokyo, Japan) using fluorescein isothiocyanate filters (magnification × 200). Two independent experiments were performed.

Chick embryo chorioallantoic membrane assay

The ability of human and iRGD endostatin to inhibit angiogenesis *in vivo* was first tested in a chick CAM assay. Three-day-old fertilized White Leghorn eggs were incubated at 37°C for 4 days, with rotation every day. A window (1 × 2 cm) was gently cut on day 7. On day 9, a small piece of paper (0.5 cm length, 0.5 cm width) was placed on the CAM. A measure of 10 μg of endostatin and iRGD endostatin were added on the paper every day for 3 days. Control CAMs were treated similarly with sterile saline. At the end of the experiment, CAMs were fixed with 10% neutral-buffered formalin and photographed using a digital camera.

Endostatin iRGD-distribution analysis *in vivo*

Mice bearing H22 tumors were intravenously injected with the endostatin iRGD at an endostatin dose equivalent to 9 mg/kg per injection. After 3 h, the mice were perfused through the heart and tissues of interest were harvested. The tissues were homogenized in cold radioimmunoprecipitation assay buffer (Sigma-Aldrich, Steinheim, Germany) containing protease inhibitors (complete miniEDTA free) and kept on ice for 30 min. The samples were then centrifuged for 30 min at 14 000 rpm. The endostatin iRGD concentration in the supernatant was quantified with enzyme-linked immunosorbant assay. Endostatin iRGD was captured with a human endostatin antibody (Novus Biologicals, Littleton, Colorado, USA), coated on a 96-well plate and detected with a human albumin antibody labeled with biotin (Invitrogen, USA).

In-vivo tumor growth-inhibition study

Female athymic nude mice (6–8 weeks old) were obtained from the Weitong Lihua Laboratory Animal Company (Beijing, China) and acclimatized to local conditions for 1 week. Logarithmically growing human liver carcinoma H22 cells were harvested by trypsinization and suspended in fresh medium at a density of 1×10^7 cells/ml. A volume of 100 μl of the single-cell suspension was then subcutaneously injected into the flanks of mice. When the tumors became visible (3 days after inoculation), mice were randomized ($n = 5$ for each group). The mice were treated with endostatin or iRGD endostatin at 20 mg/kg per day for 12 days. A control group of mice ($n = 5$) were treated with sterile PBS under similar conditions. All injections were administered subcutaneously near the neck, approximately 2 cm away from the growing tumor mass. Tumor growth was monitored by periodic caliper measurements. Tumor volume was calculated by the following formula:

$$\text{Tumor volume } (\text{mm}^3) = (a \times b^2)$$
$$2\ (a = \text{length in mm},\ b = \text{width in mm},\ a > b).$$

Statistical significance between control and treated groups was determined by repeated measurement of analysis of variance.

Results

Cloning, expression, and purification of iRGD endostatin

As shown in Fig. 1a, the recombinant fusion proteins were produced in *E. coli* at up to 23% of the total cell proteins and most of the fusion proteins were detected as inclusion bodies. To reduce the effect of contaminants on the refolding yield, inclusion bodies were washed extensively with Tris/HCl and Triton X-100 to reach more than 80% purity. The dissolved inclusion bodies were then subjected to slow dilution into the refolding buffer, which could inhibit protein aggregation, resulting in an enhanced refolding yield. The final product of endostatin–G_4S–iRGD was 85 mg/l of cell culture. The purity of the fusion proteins was more than 95%, evaluated by SDS-PAGE (Fig. 1a). The molecular weight of endostatin–G_4S–iRGD was 24 kDa, which was consistent with the size deduced from its coding sequence. Western blot analysis showed that endostatin–G_4S–iRGD reacted with monoclonal human antibodies against human endostatin (Fig. 1b).

iRGD endostatin increases endothelial cell attachment *in vitro*

To determine whether the addition of the iRGD motif to endostatin could enhance its binding to endothelial cells, cell-attachment assays were performed. As a positive control, 0.2% gelatin-coated wells were used. The number of cells attached to gelatin-coated wells was considered as 100% to calculate relative binding. HUVEC attached to endostatin-coated wells (Fig. 2). Bovine serum albumin-blocked wells were used as a negative control. In this assay system, endostatin-coated wells showed 64% cell attachment. The iRGD endostatin showed approximately 86% cell attachment.

Inhibition of endothelial cell proliferation

To determine whether the modification of human endostatin affects its biological activity, endothelial cell-proliferation

Fig. 1

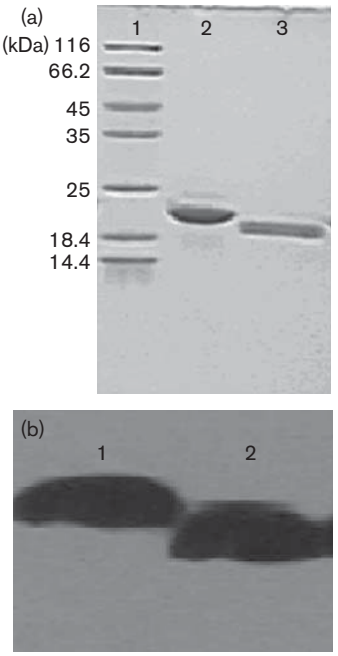

(a) Coomassie-stained 15% SDS-polyacrylamide gel electrophoresis (PAGE; nonreduced) analysis of internalization RGD (iRGD) endostatin proteins. Lane 1 shows the protein marker and lane 2 refers to iRGD endostatin protein expression plasmid carrying BL21 bacteria after induction with isopropyl β-D-1-thiogalactopyranoside to express the protein. Lane 3 shows recombination human endostatin. (b) iRGD endostatin proteins detected by western blot analysis. After SDS-PAGE, proteins were transferred to nitrocellulose membranes. Immunodetection was achieved by using human monoclonal antibody against human endostatin as primary antibody and alkaline phosphatase-conjugated antihuman immunoglobulins as secondary antibody. The phosphatase reaction was performed using NBT/BCIP (Roche, Indianapolis, Indiana, USA). Lane 1 shows the iRGD endostatin proteins and lane 2 refers to recombination human endostatin.

Fig. 2

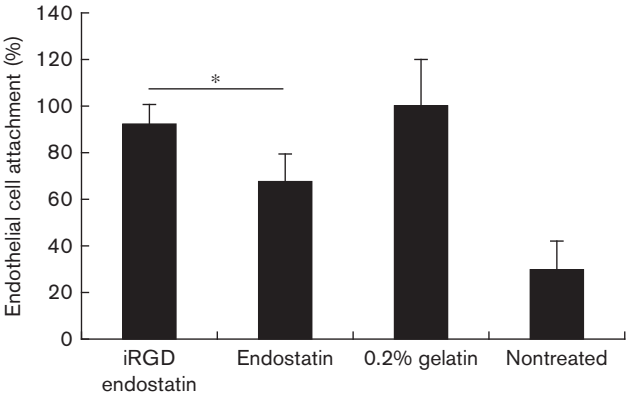

Improved endothelial cell attachment by internalization RGD (iRGD) sequence. Human umbilical vein endothelial cells prelabeled with 5-(and-6)-carboxyfluorescein diacetate/succinimidyl ester were added into triplicate wells coated with iRGD and human endostatin at a concentration of 1 nmole per well or 0.2% gelatin. Cells were quantified using a fluorescence plate reader. Data are expressed as mean (columns) ± standard deviation (bars). Statistical significance was determined using Student's *t*-test. $*P < 0.05$.

assays were performed by bromodeoxyuridine (BrdU) incorporation. Inhibition of bFGF-induced proliferation was determined in the presence of different concentrations of human and iRGD endostatin preparations. Data (Fig. 3) showed that at 1 μmol/l, endostatin inhibited bFGF-induced bovine capillary endothelial cell proliferation by 44%, which was similar to findings in a previous study [12]. Addition of the iRGD motif at the carboxyl terminal end of the endostatin further enhanced the basal antiproliferative activity. Modification of endostatin showed 85% inhibition of bFGF-induced proliferation. Interestingly, iRGD modification at the C terminal end was much more effective and completely inhibited bFGF-induced BrdU incorporation into DNA (100%).

Increased inhibition of endothelial cell migration by endostatin containing the iRGD motif

To evaluate whether the iRGD motif can affect the ability of endostatin to inhibit endothelial cell migration, transwell chamber-based migration assays were performed (Fig. 4). VEGF was used to induce endothelial cell migration. Endostatin treatment at 50 nmol/l inhibited VEGF-induced migration by 51%. In relation to this, iRGD endostatin showed statistically significant improvement in the inhibition of cell migration. Cultures treated with iRGD endostatin showed an almost complete inhibition (97%) of VEGF-induced cell migration. These results suggested that the iRGD should be an integral part of endostatin to inhibit endothelial cell migration better.

Inhibition of chick embryo chorioallantoic membrane assay

To study in-vivo antiangiogenic activity, human and iRGD endostatin were tested using a CAM assay. This assay system is based on developmental angiogenesis and is used to obtain an initial indication of angiostatic activity before testing in-vivo tumor growth models. In a modified CAM assay, 3-day-old fertilized eggs were used. Human and iRGD endostatin were applied directly on the CAM. In this assay system, human and iRGD endostatin inhibited the development of new embryonic blood vessels without affecting preexisting vasculature. IRGD endostatin inhibits the tumor activity more than endostatin (Fig. 5).

Endostatin iRGD is largely distributed at tumor tissue

To analysis whether the addition of the iRGD motif to endostatin could enhance its distribution at tumor tissue, drug distribution assays were performed. As shown in Fig. 6, endostatin distribution in the tumor, pancreas, kidney, brain, liver, spleen, and lung tissue was similar; however, after conjugation of iRGD onto endostatin, the endostatin distribution volume was significantly higher in tumor, than in other organs. However, the

distribution volume of iRGD endostatin was close to zero in the liver, spleen, and pancreas tissue. Distribution volume of iRGD endostatin compared with endostatin showed very significant statistical differences in tumor. At the same time, except for endostatin iRGD having a slightly higher distribution volume than endostatin in kidneys, the distribution within other organizations is lower than the amount of endostatin.

Fig. 3

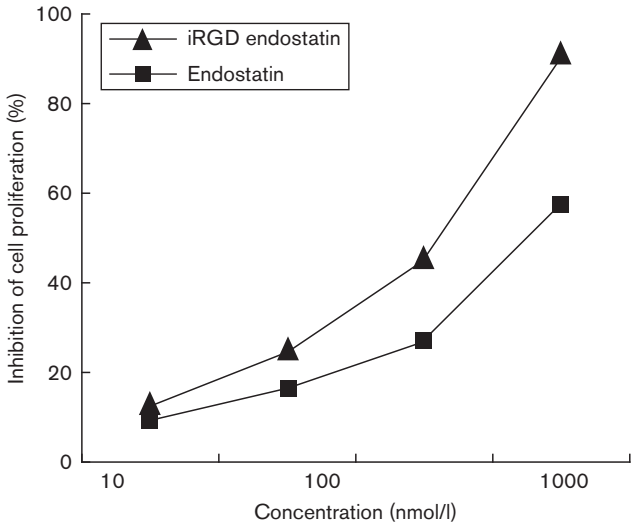

Inhibition of endothelial cell proliferation. Internalization RGD (iRGD) endostatin and endostatin were added to bovine capillary endothelial cultures treated with basic fibroblast growth factor (5 ng/ml) for 4 days and counted by the (3-(4,5-dimethylthiazol-2-yl)-2, 5-diphenyltetrazolium bromide method.

Fig. 4

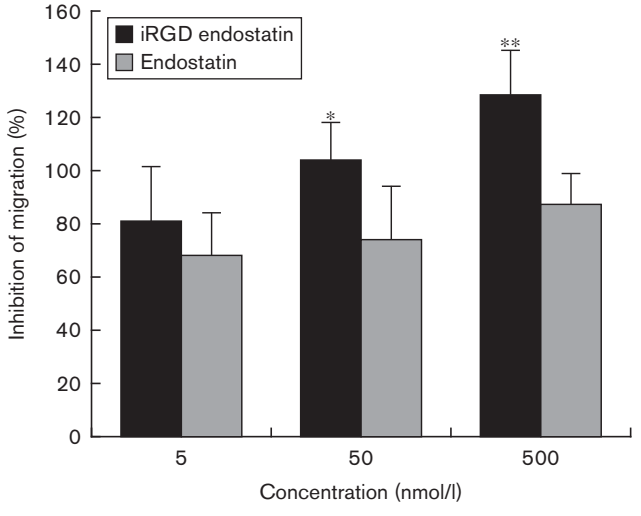

Improved inhibition of endothelial migration by internalization RGD (iRGD) modification. Effect of endostatin and iRGD endostatin on endothelial cell (human umbilical vein endothelial cells) migration was determined using transwell chambers. Vascular endothelial growth factor (25 ng/ml) was used to induce migration of endothelial cells (*$P<0.05$; **$P<0.01$).

Inhibition of liver cancer growth by injection of iRGD endostatin

To test whether iRGD modification of endostatin could improve antitumor activity, we used first an H22 xenograft model system. H22 tumors grow very fast and were allowed to establish within 3 days. At this time, small palpable tumor nodules could be easily observed. Mice were then randomized into groups. Endostatin and iRGD endostatin were administered subcutaneously at a dose of 20 mg/kg per day for a period of 12 days. As shown in Fig. 7, iRGD endostatin inhibited tumor growth significantly better than endostatin. In this model system, the control tumors reached a size of approximately 600 mm^3 by day 15. Endostatin treatment inhibited the tumor growth by approximately 30% under the conditions tested. In contrast, the tumor growth was significantly decreased by 70% in groups of animals treated with iRGD endostatin when compared with the controls.

Discussion

Endostatin is a 20 kDa, C terminal fragment of 183 amino acid residues derived from collagen XVIII [2]. In 1971, Folkman *et al.* [13] showed that tumor growth and reproduction relies on angiogenesis. Tests show that tumor growth requires neovascularization to provide nutrients and transport metabolites [14,15]. Blocking the formation of new blood vessels is an effective means to inhibit tumor growth and metastasis. Accordingly, investigators began to inhibit angiogenesis to treat cancer, which has opened a new direction. Endostatin is regarded as the most effective tumor angiogenesis inhibitor, and has become the most promising antiangiogenesis drug and research focus.

Tumor vasculatures express high levels of $\alpha_V\beta_3/\alpha_V\beta_5$ and $\alpha_5\beta_1$ integrins. Peptides containing the RGD (Arg-Gly-Asp) sequence, which is present in ligands of integrins, are effective in targeting therapeutic reagents to tumor vascular endothelium [16]. Some of the RGD peptides show impressive results in preclinical animal models [16,17]. Of the integrins $\alpha_v\beta_3/\alpha_5\beta_1$ known to interact with endostatin, binding to $\alpha_5\beta_1$ seems to be biologically relevant. However, endostatin does not have an RGD sequence. Therefore, RGD-mediated direct binding of endostatin is not possible. It is possible that endostatin forms a complex with a matrix protein, which may contain a surrogate RGD moiety, which interacts with integrins [17]. Further studies are necessary to characterize this interaction. Independent binding to $\alpha_V\beta_3/\alpha_V\beta_5$ integrins can affect biological activity. Indeed, when endostatin was modified with the iRGD sequence, there was increased binding to endothelial cells. iRGD homes to tumors by initially binding to $\alpha_v\beta_3/\beta_5$ integrins that are specifically

Fig. 5

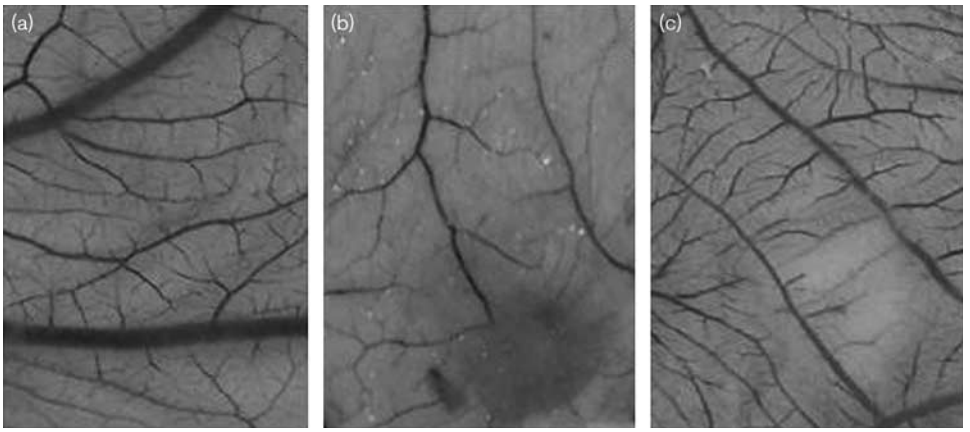

Antiangiogenic effect of internalization RGD (iRGD) and human endostatin on the chorioallantoic membrane (CAM) assay. A measure of 10 μg of human and iRGD endostatin in 50 ml of sterile saline was applied onto the CAMs every day for 3 days. Control CAMs received sterile saline. (a), control; (b), iRGD endostatin; and (c), human endostatin.

expressed on the endothelium of tumor vessels [18]. iRGD endostatin is then proteolytically cleaved in the tumor to produce endostatin CRGDK/R. The truncated protein loses much of its integrin-binding activity, but gains affinity for neuropilin-1 because of the C terminal exposure of a conditional C end Rule motif (R/KXXR/K) [19–22]. The NRP-1 binding triggers tumor and tissue penetration, which is tumor specific, because the cleavage requires previous binding of the peptide to integrins [16]. These features confer a tumor-specific tissue penetration activity on iRGD. In this study, we explored whether the iRGD peptide can enhance endostatin delivery and activity when it is fused with endostatin. This would be advantageous because it can improve the efficacy of already approved antitumor drugs. The iRGD peptide follows a multistep tumor-targeting mechanism. The intact peptide binds to the surface of cells expressing $\alpha_v\beta_3/\beta_5$ integrins, where it is proteolytically cleaved to produce the CRGDK fragment. This fragment then binds to NRP-1 and penetrates into tumor cells and tissues [23].

Enhanced endostatin permeability and tumor targeting can potentially improve the inhibition of tumor growth. Tumor models are used to assess the effect of iRGD endostatin. H22 liver cancer cells form rapidly growing tumors in athymic mice. In this model system, administration of iRGD endostatin showed a significant improvement in tumor-growth inhibition when compared with unmodified endostatin given at similar doses. The iRGD motif also improved the ability of endostatin to inhibit endothelial cell proliferation and migration. These differences can be attributed to the iRGD peptide sequence. These studies show that addition of a tumor vascular targeting and improved permeability sequence to endostatin further improves its biological activity. The iRGD sequence facilitates tumor targeting and permeability. Enhanced biological activity in combination with improved pharmacological properties significantly potentiated the antitumor effect of endostatin.

Fig. 6

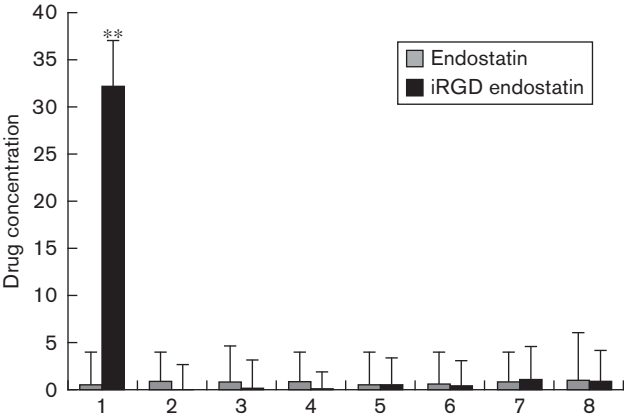

Endostatin internalization RGD (iRGD) quantification in orthotopic H22 xenograft models. Endostatin iRGD or endostatin was intravenously injected into mice with tumor 3 h earlier and captured from tumor extracts with an endostatin antibody, followed by detection with a human albumin antibody. $n=3$ for each group. Statistical analyses were carried out with Student's *t*-test in the experiment (**$P<0.01$)

Conclusion

The study on iRGD endostatin fusion protein has made it possible to develop a new effective targeting drug to fight solid tumors. We are currently investigating the activity of iRGD endostatin on the targeting of human cancer. We also plan to study the drug penetration in solid tumors and pharmacodynamic aspects of iRGD endostatin to ensure improved clinical usage.

Fig. 7

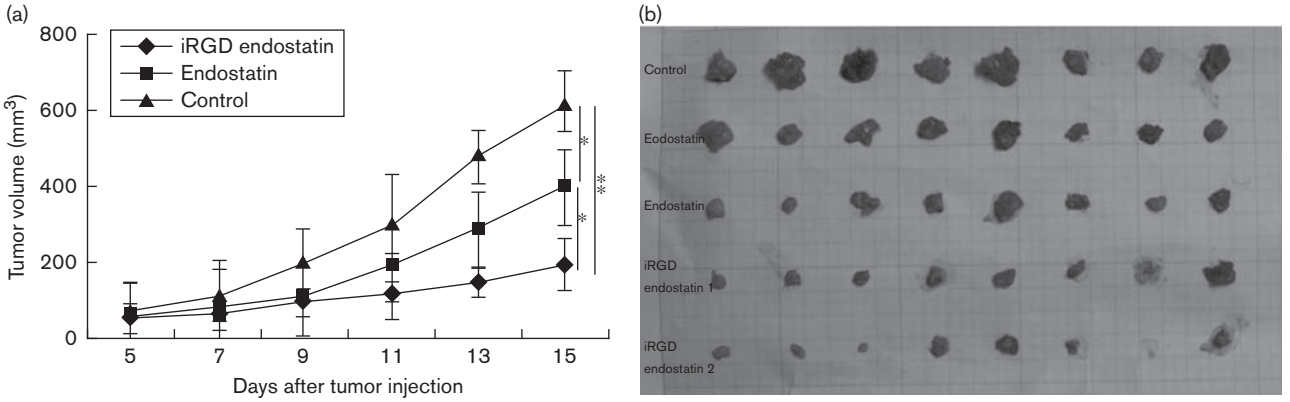

Improved inhibition of human liver cancer growth by internalization RGD (iRGD) endostatin. Human liver carcinoma cell line H22 was injected subcutaneously into female athymic mice. After tumor establishment (3 days), mice were randomized and treated with iRGD endostatin and endostatin subcutaneously about 2 cm away from tumor sites at a dose of 20 mg/kg per day. Treatment was continued for 15 days. Mean tumor volume of control is shown in (a). All tumors were harvested after 15 days, which is shown in (b). Statistical significance was determined by repeated measurement analysis of variance. The error bars indicate standard error (*$P<0.05$; **$P<0.01$ vs. control).

Acknowledgement

The authors thank *Medjaden* Bioscience Limited for assisting in the preparation of this manuscript. The original work reported in this paper was supported by Major New Drug Creation Science and Technology Special Project of China (grant 2009ZX09103-659).

References

1 Folkman J. Antiangiogenesis in cancer therapy: endostatin and its mechanisms of action. *Exp Cell Res* 2006; **312**:594–607.
2 Rehn M, Veikkola T, Kukk-Valdre E, Nakamura H, Ilmonen M, Lombardo C, *et al.* Interaction of endostatin with integrins implicated in angiogenesis. *Proc Natl Acad Sci USA* 2001; **98**:1024–1029.
3 Sorensen DR, Read TA, Porwol T, Olsen BR, Timpl R, Sasaki T, *et al.* Endostatin reduces vascularization, blood flow and growth in a rat gliosarcoma. *Neuro Oncol* 2002; **4**:1–8.
4 O'Reilly MS, Boehm T, Shing Y, Fukai N, Vasios G, Lane WS, *et al.* Endostatin: an endogenous inhibitor of angiogenesis and tumor growth. *Cell* 1997; **88**:277–285.
5 Sudhakar A, Sugimoto H, Yang C, Lively J, Zeisberg M, Kalluri R. Human tumstatin and human endostatin exhibit distinct antiangiogenic activities mediated by $\alpha_v\beta_3$ and $\alpha_5\beta_1$ integrins. *Proc Natl Acad Sci USA* 2003; **100**:4766–4771.
6 Wickstrom SA, Alitalo K, Keski-Oja J. Endostatin associates with integrin $\alpha_5\beta_1$ and caveolin-1, and activates Src via a tyrosyl phosphatase-dependent pathway in human endothelial cells. *Cancer Res* 2002; **62**:5580–5589.
7 Desgrosellier JS. Integrins in cancer: biological implications and therapeutic opportunities. *Nat Rev Cancer* 2010; **10**:9–22.
8 Sugahara KN, Teesalu T, Karmali PP, Kotamraju VR, Agemy L, Girard OM, *et al.* Tissue-penetrating delivery of compounds and nanoparticles into tumors. *Cancer Cell* 2009; **16**:510–520.
9 Teesalu T, Sugahara KN, Kotamraju VR, Ruoslahti E. C-end rule peptides mediate neuropilin-1-dependent cell, vascular, and tissue penetration. *Proc Natl Acad Sci USA* 2009; **106**:16157–16162.
10 Minchinton AI, Tannock IF. Drug penetration in solid tumours. *Nat Rev Cancer* 2006; **6**:583–592.
11 Ruoslahti E. Specialization of tumour vasculature. *Nat Rev Cancer* 2002; **2**:83–90.
12 Dhanabal M, Volk R, Ramchandran R, Simons M, Sukhatme VP. Cloning, expression, and in-vitro activity of human endostatin. *Biochem Biophys Res Commun* 1990; **258**:345–352.
13 Folkman J, Merler E, Abemathy C, Williams G. Isolation of tumor factor responsible for angiogenesis. *J Exp Med* 1971; **133**:275–288.
14 Arap W, Pasqualini R, Ruoslahti E. Cancer treatment by targeted drug delivery to tumor vasculature in a mouse model. *Science* 1998; **279**:377–380.
15 Dhanabal M, Ramchandran R, Volk R, Stillman IE, Lombardo M, Iruela-Arispe ML, *et al.* Endostatin: yeast production, mutants, and antitumor effect in renal cell carcinoma. *Cancer Res* 1999; **59**:189–197.
16 Pellet-Many C, Frankel P, Jia H, Zachary I. Neuropilins: structure, function and role in disease. *Biochem J* 2008; **411**:211–226.
17 Temming K, Schiffelers RM, Molema G, Kok RJ. RGD-based strategies for selective delivery of therapeutics and imaging agents to the tumour vasculature. *Drug Resist Updat* 2005; **8**:381–402.
18 Yokoyama Y, Ramakrishnan S. Addition of integrin binding sequence to a mutant human endostatin improves inhibition of tumor growth. *Int J Cancer* 2004; **111**:839–848.
19 Weide T, Modlinger A, Kessler H. Spatial screening for the identification of the bioactive conformation of integrin ligands. *Top Curr Chem* 2007; **272**: 1–50.
20 Hoffman JA, Giraudo E, Singh M, Zhang L, Inoue M, Porkka K, *et al.* Progressive vascular changes in a transgenic mouse model of squamous cell carcinoma. *Cancer Cell* 2003; **4**:383–391.
21 Joyce JA, Laakkonen P, Bernasconi M, Bergers G, Ruoslahti E, Hanahan D. Stage-specific vascular markers revealed by phage display in a mouse model of pancreatic islet tumorigenesis. *Cancer Cell* 2003; **4**:393–403.
22 Laakkonen P, Porkka K, Hoffman JA, Ruoslahti E. A tumor-homing peptide with a targeting specificity related to lynphatic vessels. *Nat Med* 2002; **8**:751–755.
23 Hambley TW, Hait WN. Is anticancer drug development heading in the right direction? *Cancer Res* 2009; **69**:1259–1262.